AIP | Physics of Fluids

Flow patterning in Hele-Shaw configurations using non-uniform electro-osmotic slip

Evgeniy Boyko, Shimon Rubin, Amir D. Gat, and Moran Bercovici

Citation: Physics of Fluids **27**, 102001 (2015); doi: 10.1063/1.4931637
View online: http://dx.doi.org/10.1063/1.4931637
View Table of Contents: http://scitation.aip.org/content/aip/journal/pof2/27/10?ver=pdfcov
Published by the AIP Publishing

PHYSICS OF FLUIDS **27**, 102001 (2015)

Flow patterning in Hele-Shaw configurations using non-uniform electro-osmotic slip

Evgeniy Boyko,[a] Shimon Rubin,[a] Amir D. Gat,[b] and Moran Bercovici[b]
Faculty of Mechanical Engineering, Technion–Israel Institute of Technology, Haifa, Israel

(Received 24 May 2015; accepted 5 September 2015; published online 1 October 2015)

We present an analytical study of electro-osmotic flow in a Hele-Shaw configuration with non-uniform zeta potential distribution. Applying the lubrication approximation and assuming thin electric double layer, we obtain a pair of uncoupled Poisson equations for the pressure and depth-averaged stream function, and show that the inhomogeneous parts in these equations are governed by gradients in zeta potential parallel and perpendicular to the applied electric field, respectively. We obtain a solution for the case of a disk-shaped region with uniform zeta potential and show that the flow field created is an exact dipole, even in the immediate vicinity of the disk. In addition, we study the inverse problem where the desired flow field is known and solve for the zeta potential distribution required in order to establish it. Finally, we demonstrate that such inverse problem solutions can be used to create directional flows confined within narrow regions, without physical walls. Such solutions are equivalent to flow within channels and we show that these can be assembled to create complex microfluidic networks, composed of intersecting channels and turns, which are basic building blocks in microfluidic devices. © *2015 AIP Publishing LLC.*
[http://dx.doi.org/10.1063/1.4931637]

I. INTRODUCTION

Electro-osmotic flow (EOF) is the motion of a liquid due to interaction of an externally applied electric field with the net charge in the diffuse part of an electrical double layer. For solid surfaces with uniform zeta potential and channel geometry, EOF is characterized by a uniform plug-like velocity profile. However, in practice, most surfaces are non-homogeneously charged to some extent, either due to manufacturing limitations or by intended design (see Refs. 1 and 2 and references therein).

EOF in capillaries with non-homogeneous zeta potential distribution has been studied thoroughly. Anderson and Idol[3] found an exact solution to EOF through a capillary with axially varying zeta potential, assuming negligible inertia and a thin Debye layer. Herr *et al.*[1] investigated, analytically and experimentally, EOF through a cylindrical capillary with an axial step change in zeta potential distribution. The authors measured experimentally the flow profile and showed good agreement with theoretical predictions. Ghosal[4] applied a lubrication approximation to investigate EOF in an infinitely long channel with slow axial variation in cross section geometry and zeta potential. Ghosal showed that the flow rate through any section can be related to a uniform cylindrical capillary with an equivalent radius and zeta potential, which are determined solely by the geometry and surface charge distribution in the channel.

Numerous works have also considered EOF between parallel plates. Ajdari[5,6] was the first to analytically study and provide a closed form solution to the two dimensional problem of EOF between an undulating plate and a flat plate with a periodic surface charge distribution. Ajdari focused his analysis on the cross section of the flow cell and demonstrated that the interaction of

[a]E. Boyko and S. Rubin contributed equally to this work.
[b]Authors to whom correspondence should be addressed. Electronic addresses: amirgat@technion.ac.il and mberco@technion.ac.il

periodic deformations of the plate with periodic distribution of zeta potential gives rise to net flow generation between the plates, even though the plates are on average electro-neutral. Focusing on flow between parallel plates, Long *et al.*[7] provided an analytical solution for the three dimensional EOF field due to arbitrary distribution of zeta potential. In particular, by taking the limit of a small gap between parallel plates, the authors obtained a solution associated with a Hele-Shaw case, deducing that a localized defect in zeta potential distribution induces long-range flow perturbations. Ajdari[8] considered a three dimensional geometry, consisting of two plates with a spatially varying gap and periodic zeta potential in one direction. By applying the lubrication theory, Ajdari formulated the Onsager matrix, which relates the applied pressure gradient and electric field to flow rate and electric current. Stroock *et al.*[9] performed an experimental study of EOF in flat shallow micro-channels having non-uniform zeta potential and compared the results with those of Ajdari[5,6] and Long *et al.*[7] Stroock *et al*. considered alternate positive and negative zeta potential patterns and demonstrated that various flow types such as multi-directional or circular flow can be generated, depending on whether the applied field is parallel or perpendicular to gradient of zeta potential.

In this work, we aim to study the potential use of such non-uniform electro-osmotic flows as a mechanism to create complex microfluidic channel networks, not requiring solid walls. In Sections II and III, we define the problem and derive a pair of uncoupled Poisson equations for the pressure and depth-averaged stream function, governed by gradients in zeta potential parallel and perpendicular to the applied electric field, respectively. In Section IV, we focus on axially symmetric zeta potential distributions and show that the flow field created is an exact dipole in the immediate vicinity of a disk with uniform zeta potential. In Section V, we show the effect of the orientation (relative to the electric field) of thin lines with uniform zeta potential on the pressure and vorticity fields. In Section VI, we study the inverse problem where the desired flow field is known and solve for the zeta potential distribution required in order to establish it. We then demonstrate that such inverse problem solutions can be used to create flows of desired directionality confined within narrow regions, without physical walls. We show that these can be assembled to create complex microfluidic networks and provide a specific example of Y-junction leading to a meandering channel.

II. PROBLEM DEFINITION

We here denote dimensional variables by tildes and normalized variables without tildes. Figure 1 presents a schematic illustration of the geometry and the relevant physical quantities. We consider creeping flow in a narrow gap between two parallel plates subjected to a uniform in-plane electrostatic field $\tilde{\boldsymbol{E}}_{\parallel}$. We employ a Cartesian coordinate system $(\tilde{x}, \tilde{y}, \tilde{z})$ whose $\tilde{x}$ and $\tilde{y}$ axes lie at the lower plane and $\tilde{z}$ is perpendicular thereto. The gap between the lower and upper plates is $\tilde{h}$. Each has an arbitrary zeta potential distribution, respectively, defined as $\tilde{\zeta}^L(\tilde{x}, \tilde{y})$ and $\tilde{\zeta}^U(\tilde{x}, \tilde{y})$, which vary over a characteristic length scale $\tilde{l}$ in the $\tilde{x} - \tilde{y}$ plane. Hereafter, we adopt the $\parallel$ and $\perp$ subscripts to denote parallel and perpendicular vector components to the $\tilde{x} - \tilde{y}$ plane, respectively.

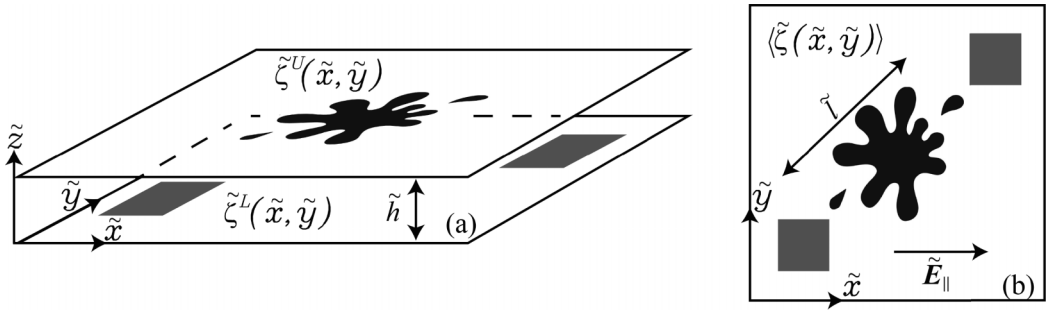

FIG. 1. Schematic illustration of the problem. (a) We consider a configuration consisting of two parallel plates, separated by a gap $\tilde{h}$. Each of the plates is functionalized with arbitrary zeta potential distribution, $\tilde{\zeta}^L(\tilde{x}, \tilde{y})$, $\tilde{\zeta}^U(\tilde{x}, \tilde{y})$, on the lower and upper plates, respectively. The fluid is subject to a uniform electric field $\tilde{\boldsymbol{E}}_{\parallel}$. (b) Averaging over the depth of the cell yields a 2D problem, in which $\langle\tilde{\zeta}\rangle$ denotes the average potential of the two plates, $\langle\tilde{\zeta}\rangle = (\tilde{\zeta}^U + \tilde{\zeta}^L)/2$.

The continuity equation for an incompressible fluid is

$$\tilde{\boldsymbol{\nabla}} \cdot \tilde{\boldsymbol{u}} = 0. \tag{1}$$

Assuming a thin electric double layer regime (see Refs. 5 and 6), the momentum equation in the bulk is given by

$$\tilde{\rho}\left(\frac{\partial \tilde{\boldsymbol{u}}}{\partial \tilde{t}} + \tilde{\boldsymbol{u}} \cdot \tilde{\boldsymbol{\nabla}}\tilde{\boldsymbol{u}}\right) = -\tilde{\boldsymbol{\nabla}}\tilde{p} + \tilde{\eta}\tilde{\nabla}^2\tilde{\boldsymbol{u}}, \tag{2}$$

where $\tilde{\boldsymbol{u}} = (\tilde{u}, \tilde{v}, \tilde{w})$ is the velocity vector, $\tilde{t}$ is time, and $\tilde{\rho}$, $\tilde{\eta}$, and $\tilde{p}$ denote the fluid density, dynamic viscosity, and pressure, respectively. We account for the body forces acting on the double layer by using the Helmholtz-Smoluchowski slip boundary conditions,[10]

$$\tilde{\boldsymbol{u}}_{\parallel}|_{\tilde{z}=0} = -\frac{\tilde{\varepsilon}\tilde{\zeta}^L\tilde{\boldsymbol{E}}_{\parallel}}{\tilde{\eta}}, \quad \tilde{\boldsymbol{u}}_{\parallel}|_{\tilde{z}=\tilde{h}} = -\frac{\tilde{\varepsilon}\tilde{\zeta}^U\tilde{\boldsymbol{E}}_{\parallel}}{\tilde{\eta}}, \quad \tilde{\boldsymbol{u}}_{\perp}|_{\tilde{z}=0,\,\tilde{h}} = 0, \tag{3}$$

where $\tilde{\boldsymbol{u}}_{\parallel} = (\tilde{u}, \tilde{v})$, $\tilde{\boldsymbol{u}}_{\perp} = \tilde{w}\hat{\boldsymbol{z}}$ and $\tilde{\varepsilon}$ is the fluid permittivity, and $\tilde{\zeta}^U$, $\tilde{\zeta}^L$ are zeta potential distribution on the upper and lower plates, respectively.

III. GOVERNING EQUATIONS FOR EOF IN A HELE-SHAW CELL WITH NON-UNIFORM ZETA POTENTIAL

Hereafter, we denote characteristic scales of the system by an asterisk superscript. The typical magnitude of the flow velocity in the $\tilde{x} - \tilde{y}$ plane, $\tilde{u}^*$, is determined by the Helmholtz-Smoluchowski slip condition as $\tilde{u}^* = -\tilde{\varepsilon}\tilde{\zeta}^*\tilde{E}^*/\tilde{\eta}$, where $\tilde{\zeta}^*$ is the characteristic value of zeta potential and $\tilde{E}^*$ is the characteristic externally applied electric field. The characteristic time scale is $t^* = \tilde{l}/\tilde{u}^*$, whereas the characteristic velocity in the $\hat{\boldsymbol{z}}$ direction, $\tilde{w}^*$, and the characteristic pressure, $\tilde{p}^*$, remain to be determined from scaling arguments.

We introduce the following normalized quantities: $(x, y, z) = (\tilde{x}/\tilde{l}, \tilde{y}/\tilde{l}, \tilde{z}/\tilde{h})$, $t = \tilde{t}/\tilde{t}^*$, $(u, v, w) = (\tilde{u}/\tilde{u}^*,\ \tilde{v}/\tilde{u}^*, \tilde{w}/\tilde{w}^*)$, $p = \tilde{p}/\tilde{p}^*$, $\zeta = \tilde{\zeta}/\tilde{\zeta}^*$, and $\boldsymbol{E}_{\parallel} = \tilde{\boldsymbol{E}}_{\parallel}/\tilde{E}^*$. We restrict our analysis to a shallow flow chamber,

$$\epsilon = \frac{\tilde{h}}{\tilde{l}} \ll 1, \tag{4}$$

and a negligible inertia regime. The latter is characterized by a negligible reduced Reynolds number, ϵRe, defined as

$$\epsilon Re = \epsilon\frac{\tilde{\rho}\tilde{u}^*\tilde{h}}{\tilde{\eta}} \ll 1. \tag{5}$$

We assume that the Dukhin number, $Du = \tilde{\sigma}_s/\tilde{\sigma}_b\tilde{l}$,[11,12] is small compared to ϵ,

$$Du = \frac{\tilde{\sigma}_s}{\tilde{\sigma}_b\tilde{l}} \ll \epsilon, \tag{6}$$

where $\tilde{\sigma}_s/\tilde{\sigma}_b$ is the ratio of surface to bulk conductivities (see Ref. 12). As noted by Yariv[13] and Khair and Squires,[14] this ratio is a length scale (also known as the healing length) which determines the spatial variations in electric fields due to non-uniformity in surface conduction. High Dukhin numbers would result in spatial variations in electric field, as well as in variations in concentration which may lead to chemiosmotic flow corrections.[15–17] Under our assumption, $Du \ll \epsilon$, the electric field and the bulk concentration can thus be considered to be uniform throughout the domain.

From order of magnitude analysis of (1) and (2), we obtain $\tilde{w}^* = \epsilon\tilde{u}^*$ and $\tilde{p}^* = \tilde{\eta}\tilde{u}^*/\epsilon^2\tilde{l}$. We note that as the flow is driven by the wall boundary conditions, the characteristic pressure is independent of the viscosity, $\tilde{p}^* = -\tilde{\varepsilon}\tilde{\zeta}^*\tilde{E}^*/\epsilon^2\tilde{l}$. Expanding the velocity field and the pressure in powers of ϵ,[18] and considering the leading order, $O(\epsilon^0)$, the normalized continuity and momentum equations (1) and (2) take the form

$$\frac{\partial u}{\partial x} + \frac{\partial v}{\partial y} + \frac{\partial w}{\partial z} = 0, \tag{7a}$$

$$\boldsymbol{\nabla}_{\parallel} p = \frac{\partial^2 \boldsymbol{u}_{\parallel}}{\partial z^2} + O(\epsilon Re, \epsilon^2), \tag{7b}$$

$$\frac{\partial p}{\partial z} = O(\epsilon^3 Re, \epsilon^2). \tag{7c}$$

Integrating (7b) twice with respect to z while making use of boundary conditions (3), we obtain an expression for the in-plane velocity field

$$\boldsymbol{u}_{\parallel} = \frac{1}{2} z\,(z-1)\,\boldsymbol{\nabla}_{\parallel} p + z\left(\zeta^U - \zeta^L\right)\boldsymbol{E}_{\parallel} + \zeta^L \boldsymbol{E}_{\parallel}, \tag{8}$$

where $\boldsymbol{\nabla}_{\parallel} = (\partial/\partial x, \partial/\partial y)$ is the two dimensional gradient. Similarly, the perpendicular velocity can be expressed as

$$\boldsymbol{u}_{\perp} = z(1-z)\boldsymbol{E}_{\parallel} \cdot \left[z \nabla_{\parallel} \zeta^U + (z-1)\nabla_{\parallel} \zeta^L\right]\hat{\boldsymbol{z}}. \tag{9}$$

Defining the mean in-plane velocity, as $\langle \boldsymbol{u}_{\parallel} \rangle = \int_{z=0}^{z=1} \boldsymbol{u}_{\parallel} dz$, and making use of (3), (7a), and (8) yield

$$\boldsymbol{\nabla}_{\parallel} \cdot \langle \boldsymbol{u}_{\parallel} \rangle = 0, \tag{10}$$

and

$$\langle \boldsymbol{u}_{\parallel} \rangle = -\frac{1}{12} \boldsymbol{\nabla}_{\parallel} p + \langle \zeta \rangle \boldsymbol{E}_{\parallel}, \tag{11}$$

where $\langle \zeta \rangle$ is an arithmetic mean value of the zeta potential on the walls, $\langle \zeta \rangle = (\zeta^U + \zeta^L)/2$. Applying the two dimensional divergence to (11), and using (10), we obtain an equation in terms of the pressure only,

$$\nabla_{\parallel}^2 p = 12 \boldsymbol{E}_{\parallel} \cdot \boldsymbol{\nabla}_{\parallel} \langle \zeta \rangle . \tag{12}$$

Similarly, applying the normal component of the curl operator to (11) leads to an equation for the stream function,

$$\nabla_{\parallel}^2 \psi = \left(\boldsymbol{E}_{\parallel} \times \boldsymbol{\nabla}_{\parallel} \langle \zeta \rangle\right) \cdot \hat{\boldsymbol{z}}, \tag{13}$$

where $\psi(x, y)$ is the averaged stream function related to the velocity field through $\langle \boldsymbol{u}_{\parallel} \rangle = (\partial\psi/\partial y, -\partial\psi/\partial x)$.

We note that (12) and (13) admit an associated gauge freedom in the choice of zeta potential, which does not affect the resulting pressure or the flow field. Specifically, for the case of an electric field acting in the $\hat{\boldsymbol{x}}$ direction, it follows that adding an arbitrary function $\zeta_{\psi}(y)$, to the zeta potential, $\langle \zeta(x, y) \rangle \to \langle \zeta(x, y) \rangle + \zeta_{\psi}(y)$, will not modify the resulting pressure in (12). Similarly, the stream function in (13) is indifferent to the transformation $\langle \zeta(x, y) \rangle \to \langle \zeta(x, y) \rangle + \zeta_p(x)$.

Equations (12) and (13) are an uncoupled set of Poisson equations for the pressure and the stream function and extend the Hele-Shaw equation[19] to include non-uniform EOF. Notably, (12) includes a source term that depends on gradients of zeta potential which are parallel to the applied electric field, while (13) relates the vorticity, $\omega = -\nabla_{\parallel}^2 \psi$, to changes of zeta potential in a direction normal to the applied electric field. In particular, in a region where the non-homogeneous term in (13) vanishes, the resulting flow field would be irrotational and a velocity potential function could be defined.

In addition to direct calculation of the flow field arising from a certain zeta distribution, we can also use (13) to obtain the required zeta potential distribution for achieving a desired flow field. Without loss of generality, we may assume that the uniform electric field is directed along the $\hat{\boldsymbol{x}}$ axis, $\boldsymbol{E}_{\parallel} = E\hat{\boldsymbol{x}}$. Solving (13) in terms of a desired stream function, we obtain the zeta potential distribution

$$\langle \zeta(x, y) \rangle = \frac{1}{E} \int \nabla_{\parallel}^2 \psi(x, y) dy + \zeta_p(x), \tag{14}$$

where $\zeta_p(x)$ is an arbitrary function of the x argument to be determined from the boundary conditions.

IV. AXIALLY SYMMETRIC ZETA POTENTIAL DISTRIBUTION

Consider the case where the zeta potential distribution acquires a non-zero value, ζ_0, in the inner region ($r_0 < r$) and vanishes in outer region, ($r_0 > r$). In the following, we adopt the superscripts *in* and *out* to distinguish between physical quantities in each one of the two regions. The corresponding zeta potential distribution is given by

$$\langle \zeta(r) \rangle = \zeta_0 H(r_0 - r), \tag{15}$$

where r is the distance as measured from the center of our coordinate system which coincides with the center of the disk, H stands for the Heaviside step function, r_0 is the radius of the disk, which here represents a characteristic length scale l, and ζ_0 is the constant value of the zeta potential in the disk.

Clearly, the abrupt change in zeta potential value described by (15) locally violates the lubrication approximation, which assumes negligible gradients in the $x - y$ plane. Nevertheless, the resulting deviations are expected to be limited to a narrow region, of order ϵ, similar to deviations near the step changes of a cross section in a long and narrow channel.[20]

For $\boldsymbol{E}_{\parallel} = (E, 0)$, (12) takes the following form in polar coordinates:

$$\frac{1}{r}\frac{\partial}{\partial r}\left(r\frac{\partial p}{\partial r}\right) + \frac{1}{r^2}\frac{\partial^2 p}{\partial \theta^2} - 12E\cos(\theta)\frac{d\langle \zeta \rangle}{dr} = 0, \tag{16}$$

where θ is the azimuthal angle in the plane and $x = r\cos(\theta)$. The last term in (16) suggests a solution of the form

$$p(r, \theta) = \alpha(r)\cos(\theta), \tag{17}$$

where $\alpha(r)$ is yet to be determined. Combining (15)-(17) yields

$$\frac{1}{r}\frac{d}{dr}\left(r\frac{d\alpha(r)}{dr}\right) - \frac{\alpha(r)}{r^2} + 12E\zeta_0\delta(r_0 - r) = 0, \tag{18}$$

where δ is the Dirac delta function. Solving (18) separately in the inner and outer regions and requiring regularity yield the following expression for the pressure:

$$p(r, \theta) = \begin{cases} \left(\dfrac{a^{out}}{r} + b^{out}r\right)\cos(\theta) \\ b^{in}r\cos(\theta) \end{cases}, \tag{19}$$

where b^{in}, b^{out}, and the dipole strength a^{out} are the coefficients to be determined from boundary conditions. Utilizing (11), (15), and (19) provides the associated closed-form expression for the flow field

$$\langle \boldsymbol{u}_{\parallel} \rangle = \begin{cases} \dfrac{1}{12}\left[\left(\dfrac{a^{out}}{r^2} - b^{out}\right)\cos(\theta)\hat{\boldsymbol{r}} + \left(\dfrac{a^{out}}{r^2} + b^{out}\right)\sin(\theta)\hat{\boldsymbol{\theta}}\right] & r_0 < r \\ \dfrac{1}{12}\left[\left(-b^{in} + 12E\zeta_0\right)\cos(\theta)\hat{\boldsymbol{r}} + \left(b^{in} - 12E\zeta_0\right)\sin(\theta)\hat{\boldsymbol{\theta}}\right] & r < r_0 \end{cases}. \tag{20}$$

In the inner region, the pressure changes linearly in the direction of the electric field, which results in a uniform velocity vector field, explicitly given by

$$\langle \boldsymbol{u}_{\parallel} \rangle^{in} = \left(-\frac{1}{12}\frac{\partial p}{\partial x} + E\zeta_0\right)\hat{\boldsymbol{x}} = \left(-\frac{1}{12}b^{in} + E\zeta_0\right)\hat{\boldsymbol{x}}. \tag{21}$$

The coefficients are determined by demanding continuity of the pressure and radial velocity component at $r = r_0$, leading to

$$a^{out} = 6E\zeta_0 r_0^2, \quad b^{in} - b^{out} = 6E\zeta_0. \tag{22}$$

The dipole strength a^{out} represents a contribution to the pressure as a result of the zeta potential in the disk, while the constant b^{out} represents the magnitude of a uniform flow field in the $\hat{\boldsymbol{x}}$ direction which stems from an externally applied pressure gradient in that direction, $b^{out} = \Delta p/\Delta x$ (e.g., for

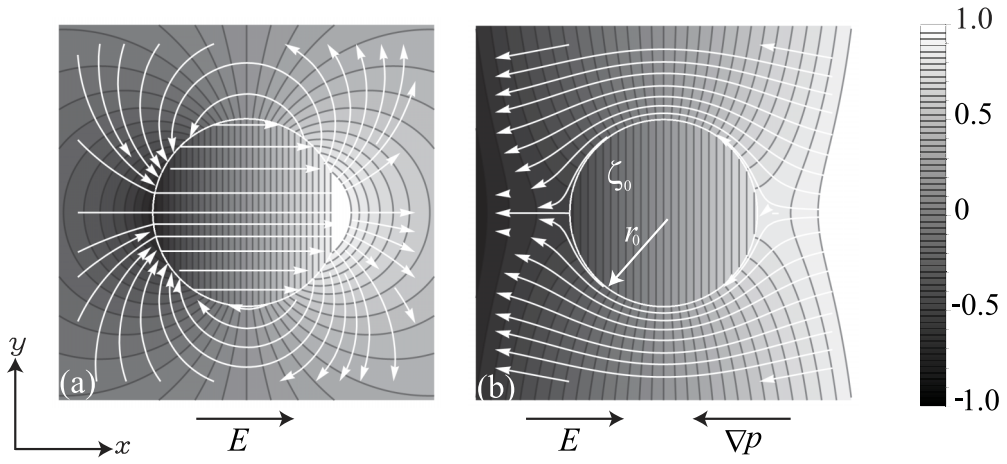

FIG. 2. The pressure distribution (colormap) and streamlines (white lines) due to a uniform electric field in the $\hat{\boldsymbol{x}}$ direction, applied to a Hele-Shaw configuration having a non-zero zeta potential in a disk of radius r_0. (a) The case of no incident flow. The depth-averaged flow field described by (20) results in a uniform flow in the inner region and dipole flow in the outer region. Note that the points of extremum pressure and vorticity correspond to locations where the source terms in (12) and (13) attain their minimal or maximal values. (b) The case where an external pressure gradient (counter-flow) is applied such that the velocity inside the disk vanishes. The result coincides with that of potential flow around a cylinder and is characterized by open streamlines which do not enter the disk region. Both solutions are normalized such that the pressure varies between ±1.

the case of constant pressure at $r \to \infty$, $b^{out} = 0$). b^{in} is then readily obtained from (22). The value of $b^{in} - b^{out}$ represents discontinuity in the $\hat{\boldsymbol{\theta}}$ component of the depth-averaged velocity on the surface $r = r_0$, induced by the vorticity sources specified by (13). From (20), we find that the corresponding jump in the $\hat{\boldsymbol{\theta}}$ component of the velocity (i.e., difference between its outer and inner values) is $-E\zeta_0$. This result can be also obtained by using the relation $\langle u_\theta \rangle = -\partial\psi/\partial r$ and integrating (13) along infinitesimal region around r_0.

While it is expected from multipole expansion theorem[21] that far from the non-uniformity the flow field will decay to a dipole,[7] we note that in this case, the flow exhibits an exact dipole behavior even in immediate vicinity of the disk.

Figure 2(a) presents the streamlines and pressure distribution map of a single electro-osmotic dipole for the case of vanishing pressure far from the disk ($b^{out} = 0$). As expected, the boundary conditions in the inner region dictate that the flow is from low pressure to high pressure while the flow in the outer region is from high pressure to low pressure. Interestingly, taking advantage of the uniform flow field in the inner region, we can superpose it with another depth-averaged flow of equal magnitude and opposite direction, to achieve zero net flow in the inner region, i.e., $\langle \boldsymbol{u}_\parallel \rangle^{in} = 0$. This can be achieved by applying a mean pressure gradient $\Delta p/\Delta x = b^{out} = 6E\zeta_0$, or by adding a bias value of $-\zeta_0/2$ to the zeta potential everywhere in the domain. Figure 2(b) presents the streamlines and pressure distribution for this case. The corresponding flow field around the disk coincides then with the well-known solution of potential flow past an infinitely long cylinder.

Employing the linearity of the governing equations enables to superpose basic dipole solution, (19), and construct axially symmetric solutions where the zeta potential, $\zeta_0(r)$, is a function of the radial coordinate. For the case in which $\zeta_0(r)$ vanishes outside a disk of radius r_0, we obtain the corresponding pressure distribution, p_{tot},

$$p_{tot}(r,\theta) = \begin{cases} \dfrac{12E\cos(\theta)}{r} \displaystyle\int_0^{r_0} \zeta_0(r_0')r_0'dr_0' & r_0 < r \\ 12E\cos(\theta)\left[\dfrac{1}{r}\displaystyle\int_0^{r} \zeta_0(r_0')r_0'dr_0' + \dfrac{r}{2}\left(\displaystyle\int_r^{r_0} \zeta_0(r_0')r_0'dr_0'\right)\right] & r < r_0 \end{cases}, \tag{23}$$

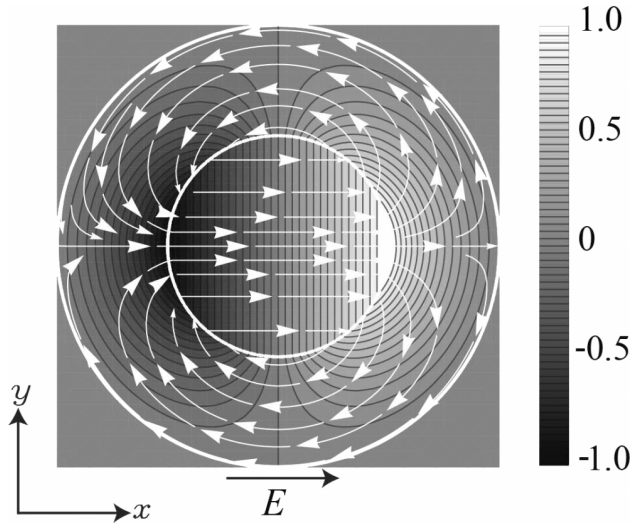

FIG. 3. Analytical solution due to superposition of two disks, described by (19) and (20), showing the superposition of two disks of radii $r_0/2$ and r_0 with zeta potentials, ζ_0 and $-\zeta_0/4$, respectively. Colormaps describe the normalized pressure distribution and the white lines show streamlines. The resultant dipole strength vanishes outside the larger disk, giving rise to a pressure and flow which are confined within the outer disk and uniform flow in the inner disk.

where the solution in the outer region corresponds again to an exact dipole, having a dipole strength $12E\int_0^{r_0}\zeta_0(r_0')r_0'dr_0'$. Figure 3 presents an analytical solution for superposition of two concentric disks of radii $r_0/2$ and r_0 with zeta potentials ζ_0 and $-\zeta_0/4$, respectively. For this special case, the pressure vanishes outside the larger disk and results in flow that is confined to the boundaries of the outer disk, whereas a uniform velocity field is obtained in the small disk, as expected.

One can also readily apply a combination of disk-shaped regions with constant zeta potential as a tool to achieve a required flow field in a Hele-Shaw cell with a uniform electric field. Specifically, as an illustration of this approach, we apply the panel method, commonly used in aerodynamics,[22] to design EOF around a symmetric NACA 0015 airfoil profile. For concreteness, we choose the direction of the electric field in our example along the $\hat{\boldsymbol{x}}$ axis and specify a known pressure gradient, $\Delta p/\Delta x$, along this direction. We place a set of 24 disks, each having a uniform (but potentially different) zeta potential, also along this axis. We then utilize the closed form dipole solution generated by each disk to calculate the velocity vector at 24 points along the airfoil curve. Demanding no-penetration at each of the points results in a set of linear algebraic equations for the associated r_0 and ζ_0 values of the disks.

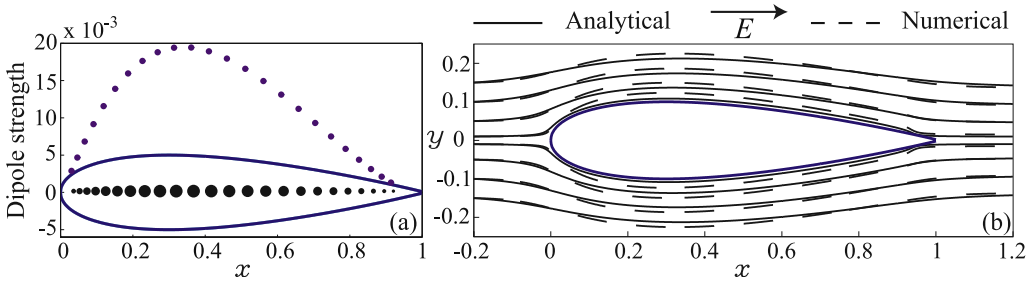

FIG. 4. Superposition of disks with uniform zeta potential enables creation of complex flow patterns, satisfying no-penetration on desired convex surfaces. (a) 24 circular disks are distributed along the $\hat{\boldsymbol{x}}$ axis. The non-dimensional dipole strength of each of the disks is set such that a no-penetration boundary condition is obtained over a NACA 0015 airfoil. (b) Comparison of analytical (solid lines) and numerical results (dashed lines) of the flow field obtained from the distribution. Analytical results were obtained from 2D Hele-Shaw model, whereas the numerical results are depth-averaged from a direct three dimensional numerical solution using Comsol Multiphysics 4.4.

Figure 4(a) shows the intensity of each of the disks as well as their location along the $\hat{\boldsymbol{x}}$ axis. Figure 4(b) presents the streamlines (solid lines) obtained from the analytical solution. To validate the results, we performed a three dimensional direct numerical simulation using Comsol Multiphysics 4.4, in which the Stokes flow equations are solved, coupled to Helmholtz Smoluchowski boundary conditions. Our grid consisted of 120 504 2$^{\text{nd}}$ order unstructured prism elements, and all solutions converged by at least seven orders of magnitude from a zero velocity initial condition. We used equally sized disks having zeta potential values as determined by the analytical solution. The velocity field is depth-averaged, and streamlines of this numerical solution are also presented in the figure (dashed lines), showing good agreement with the analytical result.

V. UNIFORM ZETA-POTENTIAL ALONG A THIN FINITE LINE

Equations (12) and (13) are both Poisson-type equations for the pressure and vorticity, in which gradients in zeta potential serve as source terms. The respective dot-product and curl operators in these source terms suggest that the solutions would depend on the geometry of surface patterning. To further highlight the roles of these source terms, let us consider two simple cases of EOF arising from a thin finite line with uniform zeta potential which is either aligned with the electric field or perpendicular to it. In both cases, we model the lines using the linearity of the governing equations and sum up the pressure contributions of dipoles having a strength per unit length a^{out}

$$dp(x,y) = \frac{a^{out}(x - x_0(l))}{(x - x_0(l))^2 + (y - y_0(l))^2} dl, \tag{24}$$

where the dipole position is parametrized by l, and dl is an infinitesimal interval along the curve l. We then use (11) to derive the fluid velocity profile outside the dipole distribution.

For the case of a line of dipoles directed along the electric field, the pressure distribution and the mean velocity are given by

$$p(x,y) = a^{out} \ln\left(\frac{r_-}{r_+}\right), \tag{25a}$$

$$\langle \boldsymbol{u}_{\parallel} \rangle = -\frac{a^{out}}{12}\left(\frac{\hat{\boldsymbol{r}}_-}{r_-} - \frac{\hat{\boldsymbol{r}}_+}{r_+}\right), \tag{25b}$$

where $\hat{\boldsymbol{r}}_\pm$ are unit vectors pointing from the observation point (x, y) to the edge points (x_-, y_0) and (x_+, y_0), and $r_\pm = \sqrt{(x - x_\pm)^2 + (y - y_0)^2}$ are the corresponding distances between these points. For a case where the line connects the points (x_0, y_-) and (x_0, y_+), and is perpendicular to the electric field, the pressure distribution and the mean velocity are given by

$$p(x,y) = a^{out}\left(\tan^{-1}\left(\frac{y - y_-}{x - x_0}\right) - \tan^{-1}\left(\frac{y - y_+}{x - x_0}\right)\right), \tag{26a}$$

$$\langle \boldsymbol{u}_{\parallel} \rangle = \frac{a^{out}}{12}\left(\frac{\hat{\boldsymbol{\theta}}_+}{r_+} - \frac{\hat{\boldsymbol{\theta}}_-}{r_-}\right), \tag{26b}$$

where $\hat{\boldsymbol{\theta}}_\pm$ are unit vectors which are perpendicular to $\hat{\boldsymbol{r}}_\pm$.

Solutions (25a) and (25b) can be interpreted as a sink and a source, located at the edges of the uniform zeta potential line. Figure 5(a) presents the resulting pressure and velocity field for this case. Clearly, the apparent violation of continuity, $\nabla_{\parallel} \cdot \langle \boldsymbol{u}_{\parallel} \rangle = 0$, at the two points is an artifact of the fact that (25a) and (25b) represent the flow outside the array of dipoles, and additional flow that connects (x_-, y_0) and (x_+, y_0) exists within this array. Note that in this case, all zeta potential gradients are in the direction of the electric field, and thus, consistent with streamlines equation (13), the flow field (25b) is free of vorticity. Solutions (26a) and (26b) are effectively equivalent to a pair of equal strength and opposite sign vortices, centered at the edges of the dipole line. Figure 5(b) presents the exact analytical solution for the pressure and velocity, as given by (26a) and (26b). Consistent with (12), high pressure gradients are formed between the two sides of the line, where the zeta potential changes in a direction parallel to electric field. At the line's edges, the pressure difference results in

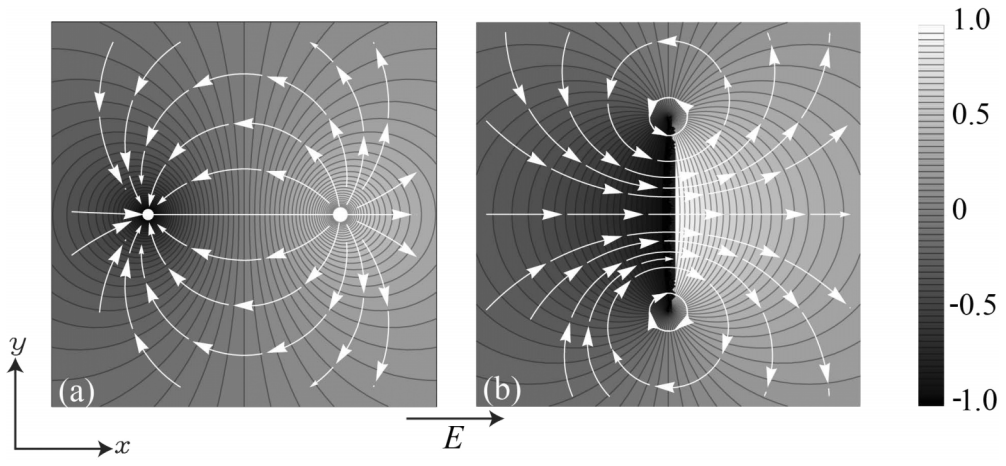

FIG. 5. Analytical solution showing the flow field due to a line of uniform zeta potential aligned (a) along the direction of the electric field and (b) perpendicular to the electric field. Each solution is obtained from superposition of dipoles, according to (24). Colormaps describe the normalized pressure distribution and the white lines show streamlines. In configuration (a), gradients in zeta potential are all in the direction of the electric field, resulting in source/sink terms at the edges of the line for pressure equation (12). Streamlines equation (13), on the other hand, remains homogeneous and no vorticity is formed. In (b), the lines edges form a zeta potential gradient perpendicular to the electric field, resulting in vorticity and localized circulation around each for the edges. In addition, a pressure difference forms across the line, reflecting the fact that the zeta potential changes in a direction parallel to the direction of the electric field.

circulatory flow, again consistent with (13) which predicts vorticity where the zeta potential changes in a direction normal to electric field (in this case, the uniform zeta line terminating into the zeta-free surface). The circulation, defined as the line integral, $\Gamma_{\pm} = \oint \langle \boldsymbol{u}_{\parallel} \rangle \cdot d\boldsymbol{l}$, along a closed path around each edge point coincides (up to a factor of $\pi/6$) with individual dipole strength $\Gamma_{\pm} = \pm \pi a^{out}/6$. Clearly, $\Gamma_{+} + \Gamma_{-} = 0$, i.e., the total circulation remains zero. More generally, from (13), it follows that the total vorticity generated by non-homogeneity of an arbitrary shape which hosts a constant zeta potential must vanish: the component of the zeta potential gradient perpendicular to the electric field is $\langle \zeta \rangle \sin(\theta)$, and thus, its line integral along the closed curve must vanish.

VI. ZETA POTENTIAL DISTRIBUTION DEFINED BY A REQUIRED FLOW FIELD AND ITS APPLICATION TO CREATE COMPLEX MICROFLUIDIC NETWORKS

In Sections IV and V, the zeta potential distribution geometry was predefined and then solved to obtain the flow field. More complex flow fields were obtained by superposing solutions. Here, we focus on obtaining the zeta potential distribution required in order to establish a desired flow field. This approach enables to generate depth-averaged flow fields which cannot be created using external pressure actuation at the boundaries. This is done by setting a desired stream function and using (14) to calculate the required zeta potential distribution. Without loss of generality, we here assume that the uniform electric field is directed along the $\hat{\boldsymbol{x}}$ axis, $\boldsymbol{E}_{\parallel} = E\hat{\boldsymbol{x}}$.

We illustrate this approach by considering flow in a square domain $[0,1] \times [0,1]$, where $x = 0$, 1 and $y = 0$ correspond to impermeable walls, and $y = 1$ corresponds to a surface of constant pressure (see Figure 6(a)). An example of such a flow is given by the stream function,

$$\psi(x, y) = y \sin(\pi x), \tag{27}$$

describing a U-shaped flow (see solid streamlines in Figure 6(a)) in which the flow enters and exits the same $y = 1$ face. Utilizing (14) and (27) yields the corresponding expression for the zeta potential

$$\langle \zeta(x, y) \rangle = -\frac{\pi^2}{2E} y^2 \sin(\pi x) + \zeta_p(x). \tag{28}$$

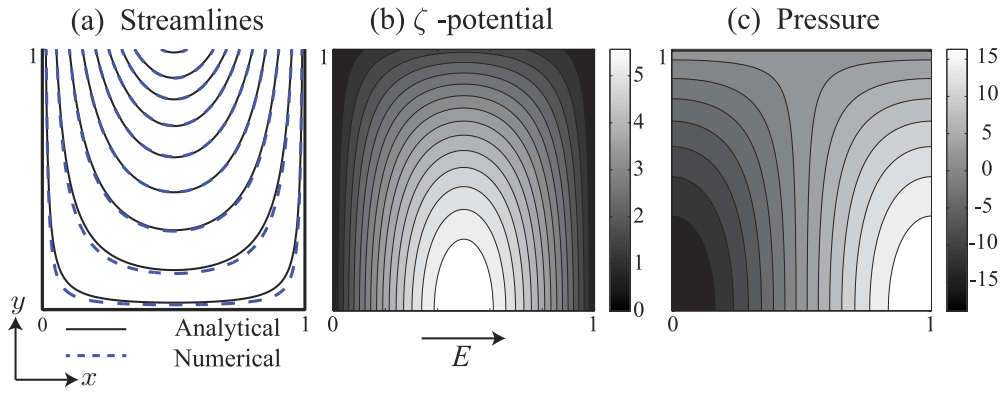

FIG. 6. Demonstration and numerical validation of the inverse problem in which the zeta potential distribution is calculated from a desired flow field. (a) Comparison of the desired streamlines (solid lines) with the depth-averaged streamlines obtained from a three dimensional numerical simulation (dashed lines). (b) Analytical zeta potential distribution, (30a), obtained in order to generate the desired flow field. (c) Resulting pressure distribution (30b). All calculations are performed using $E = 1$.

Defining the normal and tangential unit vectors to the domain boundaries as $\hat{\boldsymbol{n}}$ and $\hat{\boldsymbol{t}}$, respectively, the no-penetration boundary condition $\boldsymbol{\nabla}_{\parallel}\psi \cdot \hat{\boldsymbol{t}} = \langle \boldsymbol{u}_{\parallel} \rangle \cdot \hat{\boldsymbol{n}} = 0$ is automatically satisfied by stream function (27) on $x = 0, 1$ and $y = 0$. To satisfy the constant pressure condition, $\boldsymbol{\nabla}_{\parallel} p \cdot \hat{\boldsymbol{t}} = 0$, on the face $y = 1$, we utilize the gauge freedom in the choice of the function $\zeta_p(x)$. Substituting this condition into (11) results in $\langle \boldsymbol{u}_{\parallel} \rangle \cdot \hat{\boldsymbol{x}} = \langle \zeta \rangle |_{y=1} E$. Expressing the velocity in terms of the stream function and substituting the expression for zeta potential (28) lead to

$$\zeta_p(x) = \frac{1}{E}\left(1 + \frac{\pi^2}{2}\right)\sin(\pi x). \tag{29}$$

Consequently, the corresponding zeta potential distribution and the pressure are

$$\langle \zeta(x, y) \rangle = \frac{1}{2E}\left[\pi^2\left(1 - y^2\right) + 2\right]\sin(\pi x), \tag{30a}$$

$$p(x, y) = 6\pi\left(y^2 - 1\right)\cos(\pi x), \tag{30b}$$

and are presented in Figures 6(b) and 6(c), respectively.

To validate the results, we compare the desired flow field (27) with the flow field obtained by numerically solving a three dimensional case in which resulting zeta potential (30a) is used in the slip boundary conditions on both the lower and upper walls. To solve the corresponding Stokes equations, we used the creeping flow package in Comsol Multiphysics 4.4. Streamlines of the depth-averaged velocity field are presented in Figure 6(a) (dashed lines), showing good agreement with the desired flow.

We now turn to illustrate the use of (14) to engineer complex flow fields of the type encountered in microfluidic devices. These flows are typically confined to narrow channels composed of turns, junctions, and straight segments. Importantly, in our approach, there are no real walls that confine the liquid and yet, using appropriate zeta potential, the fluid achieves desired directionality within specific regions of interest, and its velocity strongly decays outside them. We show that under certain conditions, the corresponding zeta potential distribution necessary to generate complex flow fields of such type admits modularity, i.e., can be represented as a sum of simple and basic distributions which allow sufficiently smooth matching.

First, we wish to determine the zeta potential necessary to generate a flow field along a curve $y = f(x)$, under a homogeneous electric field. We set a stream function of the form

$$\psi(x, y) = F(y - f(x)) \equiv F(\chi), \tag{31}$$

which ensures that ψ has a constant value along $y = f(x)$ for any choice of F. The variable $\chi = y - f(x)$ parametrizes different streamlines according to their displacement along the $\hat{\boldsymbol{y}}$ axis.

By definition of the stream function, and using (31), the velocity components can be expressed as

$$\langle u\rangle = \frac{\partial \psi}{\partial y} = F'(\chi), \quad \langle v\rangle = -\frac{\partial \psi}{\partial x} = f'(x)F'(\chi). \tag{32}$$

To determine the zeta potential necessary to generate flow field (32), we substitute stream function (31) into relation (14) which yields the following closed form expression for the necessary zeta potential:

$$\langle \zeta(x,y)\rangle = \frac{1}{E}\left(F'(\chi) + f'(x)^2F'(\chi) - F(\chi)f''(x)\right) + \zeta_p(x), \tag{33}$$

where $\zeta_p(x)$ is an arbitrary function. Hereafter, we focus on a case where $\zeta_p(x) = 0$. Utilizing (32) and polar representation of the flow field components, $\langle u\rangle = \left|\langle \boldsymbol{u}_{\parallel}\rangle\right|\cos(\theta)$ and $\langle v\rangle = \left|\langle \boldsymbol{u}_{\parallel}\rangle\right|\sin(\theta)$, (33) is rewritten as

$$\langle \zeta(x,y)\rangle = \frac{1}{E\cos^2(\theta)}\left(\langle u\rangle - F(\chi)\frac{d\theta}{dx}\right). \tag{34}$$

This expression allows to directly obtain the zeta potential required in order to produce the desired flow, described by stream function (31). In regions where the flow direction changes significantly, the second term in (34) dominates over the first term, and vice versa in regions where the flow field is nearly unidirectional. In particular, in regions with uniform flow, the zeta potential admits a simple expression given by $\langle u\rangle/E\cos^2(\theta) = \left|\langle \boldsymbol{u}_{\parallel}\rangle\right|/E\cos(\theta)$. Also, (34) shows that the zeta potential required to generate flow in a direction perpendicular to electric field (i.e., $\langle u\rangle = 0$) diverges and is thus non-physical.

A convenient function to define a flow field in which the velocity is confined to a narrow region around the streamline $y = f(x)$ is

$$\psi(x,y;\theta_{in},\theta_{out}) = \tanh\left(\gamma\left(y - f(x;\theta_{in},\theta_{out})\right)\right). \tag{35}$$

This function exhibits significant gradients in a region of width $1/\gamma$ around the streamline. Outside of this region, it quickly reaches a negligible gradient, and thus negligible flow.

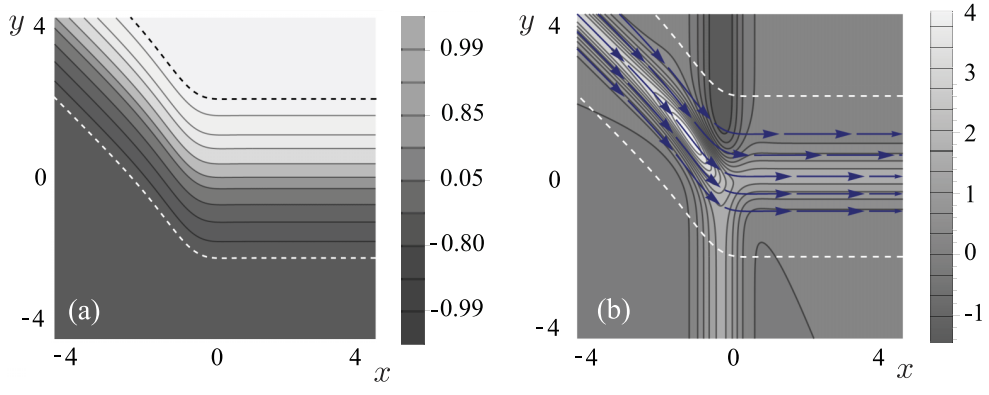

FIG. 7. Analytical example of zeta potential calculation for a bent channel segment. (a) Colormap of the stream function $\psi(x,y;-\pi/4,0)$ given by (35), which describes incoming flow at an angle $-\pi/4$ and horizontal outgoing flow. Here, $\beta = \gamma = 2$, $n = 4$, $E = 1$. The stream function is constructed of two regions having negligible gradients (and thus negligible flow), which are connected through a steep gradient region of width $1/\gamma$. The dashed lines correspond to streamlines on which the velocity drops to 1% of its maximum value, thus defining the outer boundaries of a channel. (b) Colormap of the zeta potential, necessary to generate the desired flow field (blue streamlines), obtained by inserting the corresponding stream function into (33). The pattern shows two regions of opposite values of zeta potential which extend along the line $x = 0$, towards positive and negative directions of the $\hat{\boldsymbol{y}}$ axis. This contribution stems from the term $-F(\chi)f''(x)$ in (33), and occurs in the region where $f(x)$ admits its highest second derivative. Two other regions which host significant values of zeta potential correspond to zones with nearly unidirectional flow, represented by the first term in (34).

For creation of stream function modules, which are useful for the construction of microchannel segments, it is convenient to choose the function f as

$$f(x;\theta_{in},\theta_{out}) = \tan(\theta_{in})\frac{x}{(1+\exp(\beta x))^n} + \tan(\theta_{out})\frac{x}{(1+\exp(-\beta x))^n}. \quad (36)$$

This function describes a smooth approximation of a bi-linear curve, which approaches $y = \tan(\theta_{out})\,x$ as x tends to $+\infty$ and to $y = \tan(\theta_{in})\,x$ as x tends to $-\infty$. n and β are positive parameters which set the exact shape of the curve near the bending point $(0,0)$.

Figure 7(a) presents the contour map of the stream function, $\psi(x,y;-\pi/4,0)$. The streamlines describe an incoming fluid flowing at an angle $-\pi/4$, a turn region around the origin and outgoing flow along the $\hat{\boldsymbol{x}}$ axis (zero angle). The region which supports a significant flow velocity is enclosed between the dashed lines, and its width is of order $1/\gamma$. The magnitude of the flow velocity on the dashed lines drops to 1% of its peak value. Figure 7(b) shows several streamlines (blue arrows), together with the zeta potential described by (34), necessary to generate this flow field. The second derivative of the function $\psi(x,y;-\pi/4,0)$ acquires significant values around the line $x = 0$, which

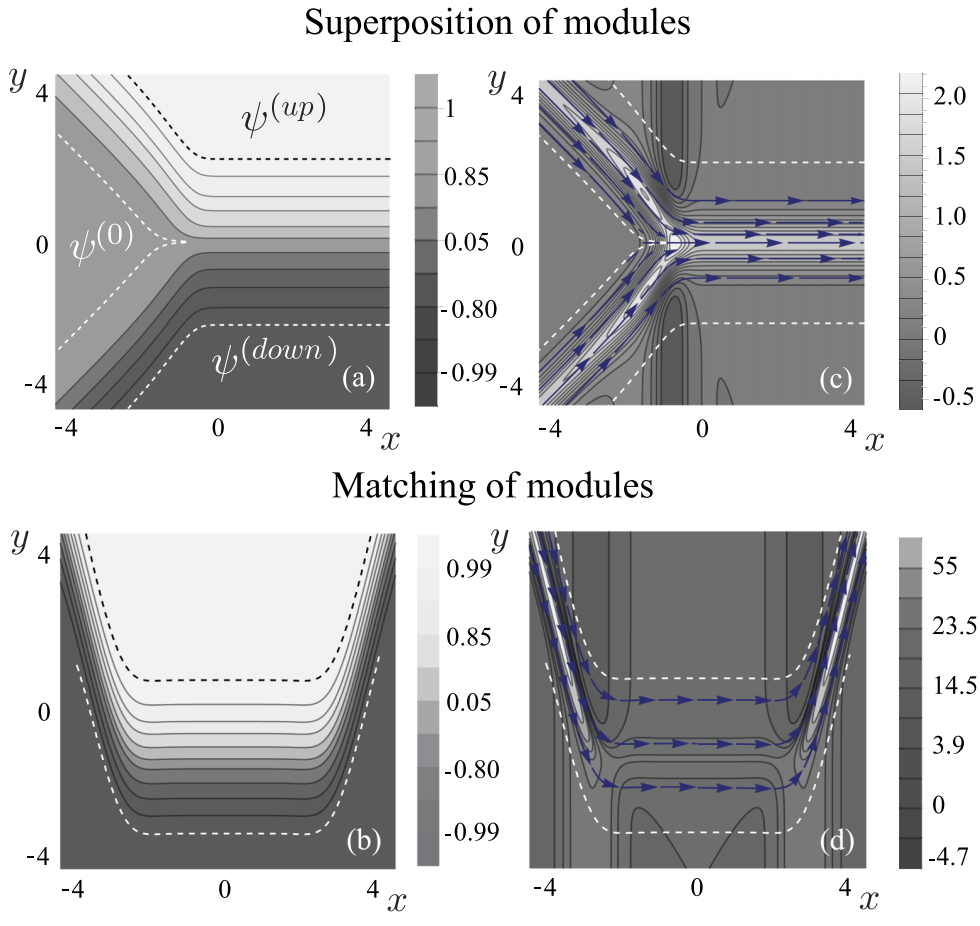

FIG. 8. Analytical examples showing superposition and matching of two basic modules. (a) Superposition assembly of the functions $1/2\psi(x,y;-\pi/4,0)$ and $-1/2\psi(x,y;+\pi/4,0)$ forming a Y-junction in which incoming flows are directed at an angle $\pm\pi/4$ and combined into a single outgoing flow along the $\hat{\boldsymbol{x}}$ axis. The value of $\psi^{(up)}-\psi^{(down)}$ determines the total flow rate in the channel, whereas modifying the value of $\psi^{(0)}$ allows to control the fraction carried by each of the two incoming flows. (b) Stream function of two modules: $\psi(x-x_1,y;-\pi/4,0)$ for $x<0$ and $\psi(x-x_2,y;+\pi/4,0)$ for $x>0$ (with $x_2=-x_1=3.5$), matched along the line $x=0$, forming U-shaped streamlines. ((c) and (d)) Colormaps of the zeta potential distributions necessary to generate the desired flow field (blue arrows) obtained by substituting the stream functions corresponding to ((a) and (b)) into (33). In all subfigures, the magnitude of flow velocity on the dashed lines drops to 1% of its peak value and the parameters which enter (33), (35), and (36) are given by $\beta=\gamma=2$, $n=4$, $E=1$.

results in a significant contribution of the $-F(\chi)f''(x) = -\psi(x,y)f''(x)$ term in (33). Since $f''(x)$ is independent of y, and since the stream function values are constant far from the channel region, this results in zeta potential values of opposite signs at $x = 0$, which extend uniformly toward $y = \pm\infty$. Far from the line $x = 0$, where the flow has a nearly uniform directionality, the first term in (34) dominates and the resulting zeta potential distribution is uniform along the incoming and outgoing flow directions.

More complex flows can be created by joining of multiple stream function modules. Figure 8(a) shows the stream function, $1/2\,(\psi(x,y;-\pi/4,0) - \psi(x,y;+\pi/4,0))$, obtained by superposition of two stream functions described by (35). In such superpositions, the resulting flux is thus the sum of individual fluxes. This allows, for example, constructing junctions where multiple incoming streams are combined into a single one. In the example shown in Figure 8(a), the resulting flow consists of incoming streamlines along the angles $-\pi/4$ and $\pi/4$ towards the origin, and a combined outgoing flow along the $\hat{\boldsymbol{x}}$ axis. We note that the total flux in the channels can be controlled by modifying the value of $\psi^{(up)} - \psi^{(down)}$, whereas the relative flux of each of the streams can be dictated by modifying the value $\psi^{(0)}$ for fixed values of $\psi^{(up)}$ and $\psi^{(down)}$. Figure 8(c) shows the zeta potential necessary to generate this flow field, obtained by substituting the corresponding stream function into (34). Note that following the same steps, one can consider a linear combination of N basic functions $\psi(x,y;\theta_n,0)$ which generates a converging flow from θ_n incoming directions and a combined flow along a single outgoing direction. Figure 8(b) presents streamlines obtained from matching the stream functions $\psi(x-x_1,y;-\pi/4,0)$ and $\psi(x-x_2,y;+\pi/4,0)$ (with $x_2 = -x_1 = 3.5$), along the common boundary

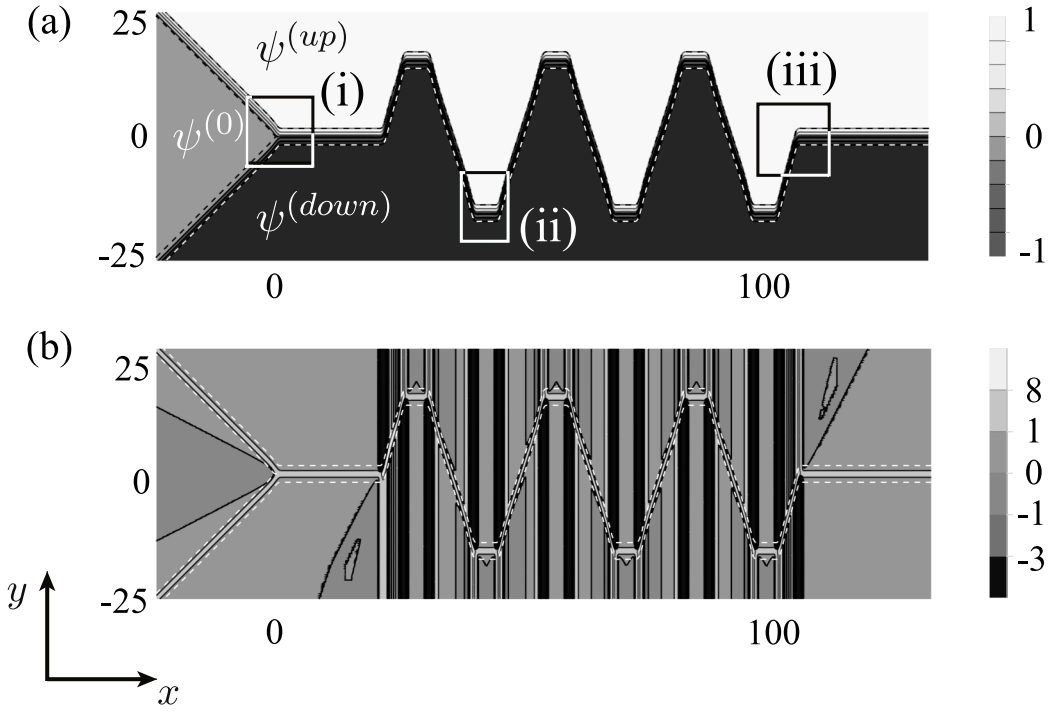

FIG. 9. Analytical example demonstrating the use of matching and superposition of basic modules for creation of a microfluidic network. (a) and (b) show the desired streamlines pattern and the zeta potential distribution necessary to generate the corresponding flow field, respectively. The microfluidic network is composed of a Y-junction, created by superposition assembly of $1/2\psi(x,y;+\pi/4,0)$ and $-1/2\psi(x,y;-\pi/4,0)$, followed by a matching assembly of $\psi(x-x_i,y-f_i;-\pi/4,0)$ and $\psi(x-x_i,y-f_i;+\pi/4,0)$ where the index i enumerates the bending points (x_i,f_i) of different basic modules, and their matching boundary lines, $x=(x_i+x_{i+1})/2$. Detailed structure of each one of the modules enclosed within the regions (i), (ii), is described in Figure 8 while region (iii) is described by a module similar to the one shown in Figure 7. In both colormaps, the magnitude of flow velocity on the dashed lines drops to 1% of its peak value and the parameters which enter (33), (35), and (36) are given by $\beta=\gamma=2$, $n=4$, $E=1$.

$x = 0$. Matching allows the construction of extended channels in which the flux in one module is preserved in the next. In this assembly, the resulting flow consists of an incoming stream along a straight line with slope $-\tan(2\pi/5)$, a short horizontal flow parallel to the $\hat{\boldsymbol{x}}$ axis, and outgoing flow along a straight line with a slope $\tan(2\pi/5)$. To join two such elements, the values of ζ and its derivative along the common boundary should ideally be matched. (34) shows that the zeta potential of streamlines directed along the electric field (zero slope) depends solely on the velocity value and angle and thus can be used for outgoing flow from one domain and incoming flow to another.

The resulting zeta potential for this type of matching is presented in Figure 8(d). While the values of the stream function and zeta potential match precisely along the common boundary, $x = 0$, their corresponding derivatives experience a discontinuity. The discontinuity in the stream function derivative, Δ, along the common boundary is given by

$$\Delta = 2\frac{1 + (1 - n\beta x)\exp(\beta x)}{(1 + \exp(\beta x))^{n+1}}, \tag{37}$$

and could be made arbitrarily small by extending the length of the domain or by proper choice of the corresponding parameters. For typical values in our example, Δ does not increase above 10^{-6}, which would be negligible in typical microfluidic systems.

Figure 9 illustrates the use of superposition and matching for creation a micromixer geometry, in which two streams merge in a Y-junction and continue to a serpentine channel consisting of six $4\pi/5$ turns. Figure 9(a) shows the stream function, which is an assembly of basic flow fields matched together along common boundaries. The magnitude of flow velocity on the dashed lines drops to 1% of its peak value. Figure 9(b) shows the necessary zeta potential distribution, obtained from (34).

VII. SUMMARY AND CONCLUSIONS

In this work, we studied EOF in a Hele-Shaw configuration, with non-uniform zeta potential distribution. We demonstrated the use of zeta potential distributions for patterning of complex flow fields, including microchannel networks.

The flow fields we obtained in this work are depth-averaged fields. Care should be taken when analyzing the flow of particles in such fields; for sufficiently high diffusivity of the particle (i.e., low Peclet number), an ensemble of particles will move with the average velocity field. However, at high Peclet, individual particles may follow particular streamlines and the ensemble will exhibit a behavior substantially different than that of the average.

In Sections IV and V, we demonstrated the construction of complex flow fields by superposition of basic solutions. We note that (11)–(13) are conformal invariant. This follows directly from the fact that these equations can be rewritten so that each term will contain equal number of gradient operators (see Ref. 23). This opens a door to employ conformal mapping machinery and to calculate resultant pressure and flow field due to non-uniform zeta potential patterning in the presence of complex geometries with real walls. It is also worth noting that governing equations (12) and (13) for the pressure and depth-averaged stream function can be extended to include the effect of slow varying height between the plates. The modified governing equation will be an EOF driven Reynolds equation in which both the viscous terms and the EOF terms depend on the spatially varying gap between the plates. While the governing equation will remain linear, and thus could potentially be resolved analytically, it is beyond the scope of this work.

In practice, surface patterning could be obtained in several ways, including chemical modification of the surface or using an array of surface electrodes. The latter adds complexity but has the potential advantage of allowing surface potentials which are much higher, as well as dynamic modification of the zeta potential distribution. Further study would be required to characterize the effect of zeta potential discretization on the resulting flow fields. Flow patterning by EOF, particularly by dynamic modification of the surface potential, may serve a powerful tool for manipulating fluids without mechanical components in a variety of microfluidic applications.

ACKNOWLEDGMENTS

This research was supported by the Israel Science Foundation (Grant Nos. 512/12 and 818/13) and FP7 Marie Curie Career Integration (Grant No. PCIG09-GA-2011-293576). S.R. is supported in part by a Technion fellowship from the Lady Davis Foundation.

[1] A. E. Herr, J. I. Molho, J. G. Santiago, M. G. Mungal, T. W. Kenny, and M. G. Garguilo, "Electroosmotic capillary flow with nonuniform zeta potential," Anal. Chem. **72**, 1053–1057 (2000).
[2] H. A. Stone, A. D. Stroock, and A. Ajdari, "Engineering flows in small devices," Annu. Rev. Fluid Mech. **36**, 381–411 (2004).
[3] J. L. Anderson and W. K. Idol, "Electroosmosis through pores with nonuniformly charged walls," Chem. Eng. Commun. **38**, 93–106 (1985).
[4] S. Ghosal, "Lubrication theory for electro-osmotic flow in a microfluidic channel of slowly varying cross-section and wall charge," J. Fluid Mech. **459**, 103–128 (2002).
[5] A. Ajdari, "Electro-osmosis on inhomogeneously charged surfaces," Phys. Rev. Lett. **75**, 755–758 (1995).
[6] A. Ajdari, "Generation of transverse fluid currents and forces by an electric field: Electro-osmosis on charge-modulated and undulated surfaces," Phys. Rev. E **53**, 4996–5005 (1996).
[7] D. Long, H. A. Stone, and A. Ajdari, "Electroosmotic flows created by surface defects in capillary electrophoresis," J. Colloid Interface Sci. **212**, 338–349 (1999).
[8] A. Ajdari, "Transverse electrokinetic and microfluidic effects in micropatterned channels: Lubrication analysis for slab geometries," Phys. Rev. E **65**, 016301 (2001).
[9] A. D. Stroock, M. Weck, D. T. Chiu, W. T. S. Huck, P. J. A. Kenis, R. F. Ismagilov, and G. M. Whitesides, "Patterning electro-osmotic flow with patterned surface charge," Phys. Rev. Lett. **84**, 3314–3317 (2000).
[10] R. J. Hunter, *Foundations of Colloid Science*, 2nd ed. (Oxford University Press, 2000).
[11] S. S. Dukhin, "Non-equilibrium electric surface phenomena," Adv. Colloid Interface Sci. **44**, 1–134 (1993).
[12] J. Lyklema, *Fundamentals of Interface and Colloid Science: Solid-Liquid Interfaces* with special contributions by A. de Keizer, B. H. Bijsterbosch, G. J. Fleer, and M. A. Cohen Stuart (Academic Press, 1995), Vol. 2.
[13] E. Yariv, "Electro-osmotic flow near a surface charge discontinuity," J. Fluid Mech. **521**, 181–189 (2004).
[14] A. S. Khair and T. M. Squires, "Surprising consequences of ion conservation in electro-osmosis over a surface charge discontinuity," J. Fluid Mech. **615**, 323–334 (2008).
[15] B. V. Deryaguin, S. S. Dukhin, and A. A. Korotkova, "Diffusiophoresis in electrolyte solutions and its role in the mechanism of film formation from rubber latexes by the method of ionic deposition," Kolloidn. Zh. **23**, 53 (1961) [B. V. Derjaguin, S. S. Dukhin, and A. A. Korotkova, "Diffusiophoresis in electrolyte solutions and its role in the Mechanism of the formation of films from caoutchouc latexes by the ionic deposition method," Prog. Surf. Sci. **43**, 153–158 (1993)].
[16] D. C. Prieve, J. L. Anderson, J. P. Ebel, and M. E. Lowell, "Motion of a particle generated by chemical gradients. Part 2. Electrolytes," J. Fluid Mech. **148**, 247 (1984).
[17] A. S. Khair and T. M. Squires, "Fundamental aspects of concentration polarization arising from nonuniform electrokinetic transport," Phys. Fluids **20**, 087102 (2008).
[18] G. K. Batchelor, *An Introduction to Fluid Dynamics* (Cambridge University Press, 2000), pp. 216–224.
[19] H. S. Hele-Shaw, "Flow of water," Nature **58**, 520 (1898).
[20] C. M. Brotherton and R. H. Davis, "Electroosmotic flow in channels with step changes in zeta potential and cross section," J. Colloid Interface Sci. **270**, 242–246 (2004).
[21] L. G. Leal, *Advanced Transport Phenomena: Fluid Mechanics and Convective Transport Processes* (Cambridge University Press, 2007).
[22] J. Katz and A. Plotkin, *Low-Speed Aerodynamics*, 2nd ed. (Cambridge University Press, 2001).
[23] M. Z. Bazant, "Conformal mapping of some non-harmonic functions in transport theory," Proc. R. Soc. A **460**, 1433–1452 (2004).